



## Effect of wave amplitude on turbulent flow in a wavy channel by direct numerical simulation

H.S. Yoon<sup>a</sup>, O.A. El-Samni<sup>b</sup>, A.T. Huynh<sup>c</sup>, H.H. Chun<sup>a,\*</sup>, H.J. Kim<sup>c</sup>, A.H. Pham<sup>c</sup>, I.R. Park<sup>d</sup>

<sup>a</sup> Advanced Ship Engineering Research Center, Pusan National University, San 30, Jangjeon-Dong, Gumjeong-Gu, Busan 609-735, Republic of Korea

<sup>b</sup> Mechanical Power Engineering Department, The University of Alexandria, El-Chatby, Alexandria 21411, Egypt

<sup>c</sup> Naval Architecture and Ocean Engineering, Pusan National University, San 30, Jangjeon-Dong, Gumjeong-Gu, Busan 609-735, Republic of Korea

<sup>d</sup> Maritime and Ocean Engineering Research Institute, KORDI, 171 Jang-Dong, Yuseong-Gu, Daejeon 305-343, Republic of Korea

### ARTICLE INFO

#### Article history:

Received 2 November 2007

Accepted 29 March 2009

Available online 15 April 2009

#### Keywords:

Wavy surface

Reverse flow

Separation

Drag

Immersed boundary method

### ABSTRACT

The present study numerically investigates the characteristics of three-dimensional turbulent flow in a wavy channel. For the purpose of a careful observation of the effect of the wave amplitude on the turbulent flow, numerical simulations are performed at a various range of the wave amplitude to wavelength ratio ( $0.01 \leq \alpha/\lambda \leq 0.05$ ), where the wavelength is fixed with the same value of the mean channel height ( $H$ ). The immersed boundary method is used to handle the wavy surface in a rectangular grid system, using the finite volume method. The Reynolds number ( $Re = U_b H/\nu$ ) based on the bulk velocity ( $U_b$ ) is fixed at 6760. The present computational results for a wavy surface are well compared with those of references. When  $\alpha/\lambda = 0.02$ , the small recirculating flow occurs near the trough at the instant, but the mean reverse flow is not observed. In the mean flow field, the reverse flow appears from  $\alpha/\lambda = 0.03$  among the wave amplitude considered in this study. The domain of the mean reverse flow defined by the locations of separation and reattachment depends strongly on the wave amplitude. The pressure drag coefficient augments with increasing the wave amplitude. The friction drag coefficient shows the increase and decrease behavior according to the wave amplitude. The quantitative information about the flow variables such as the distribution of pressure and shear stress on the wavy surface is highlighted.

© 2009 Elsevier Ltd. All rights reserved.

### 1. Introduction

The turbulent flow over the wavy surface has been widely experienced in the environmental and industry fields. For example, the coupling fluxes between the atmosphere and ocean occur through a wavy surface that changes spatially and temporally. While many experiments and computations have considered the solid wavy walls, the results are still of some interest for gas flows over wavy liquids, since the gas sees the liquid as something like a wavy wall (De Angelis et al., 1997).

Consequently, this problem gathered the considerable attention of many researchers (Zilker and Hanratty, 1979; Buckles et al., 1984; Kuzan, 1986; Kuzan et al., 1989; Hudson et al., 1996; Maaß and Schumann, 1996; De Angelis et al., 1997; Cherukat et al., 1998) who have carried out experiments or computations to understand the effect of the wavy surface on the flow characteristics and structures which do not appear in a flat surface.

Especially, Hudson et al. (1996) provided the extensive measurements of the turbulent characteristics such as the Reynolds stresses, turbulent intensities and production over a wavy surface with a wave amplitude ( $\alpha$ ) to wavelength ( $\lambda$ ) ratio equal to 0.05 and a Reynolds number ( $Re = U_b H/\nu$ ) of 6760 based on the bulk velocity ( $U_b$ ) and the mean height of the channel ( $H$ ). They showed that the turbulence production near the wavy surface is mainly associated with the shear layer separated from the wavy surface.

Among the several computational researches for the turbulent flow over the wavy surface, Maaß and Schumann (1996) and Cherukat et al. (1998) have been frequently referred as a benchmark case, since both researches provide plenty of turbulent quantities which were obtained by the DNS of turbulent channel flow with a wavy surface for  $\alpha/\lambda = 0.05$  and  $Re = U_b H/\nu = 6760$ . Their DNS results greatly contributed to providing a better understanding of the flow characteristics governed by the wavy surface. Also, Cherukat et al. (1998) well summarized the early analytic and numerical studies. Their principal finding is the occasional velocity bursts which originate in the separated region and extend over large distances away from the wavy wall.

\* Corresponding author. Tel.: +82 51 510 2341; fax: +82 51 581 3718.  
E-mail address: [chunahh@pusan.ac.kr](mailto:chunahh@pusan.ac.kr) (H.H. Chun).

It is now well known that the strong streamwise vortices start to appear in the upslope portion of the wave and disappear before the next crest. If the wave slope is large enough, the flow separates downstream of the crest and then unsteadily recirculates. The flow reattaches usually just downstream of the trough, and then a thin accelerating boundary layer forms.

The work being presented covers DNS simulations of flow past a fixed wavy wall, which is to be considered as a simplified model of wind flow over water waves. The present study aims at exploring the characteristics of turbulent wavy flow by increasing the wave amplitude in the range of  $\alpha/\lambda \leq 0.05$ . The main emphasis of this study is to find the critical wave amplitude where the mean reverse flow occurs. Moreover, we focus on providing the quantitative information about the flow variables, such as spatial variations of velocity, turbulent kinetic energy, Reynolds shear stress and drag coefficients according to the wave amplitude.

## 2. Numerical approach

The immersed boundary method is used to simulate three-dimensional flow over a wavy channel. Therefore, the governing equations describing unsteady incompressible viscous flow field in the present study are the momentum and continuity equations

$$\frac{\partial u_i}{\partial t} + \frac{\partial u_i u_j}{\partial x_j} = -\frac{\partial p}{\partial x_i} + \frac{1}{Re} \frac{\partial^2 u_i}{\partial x_j^2} + f_i \quad (1)$$

$$\frac{\partial u_i}{\partial x_i} - q = 0 \quad (2)$$

where  $x_i$  are Cartesian coordinates,  $u_i$  are the corresponding velocity components,  $t$  is the time and  $p$  is the pressure. The momentum forcing  $f_i$  and mass source/sink  $q$  are applied on the body surface or inside the body to satisfy the no-slip condition and mass conservation the cell containing the immersed boundary.

All the variables are nondimensionalized by the channel mean height  $H$  and bulk velocity  $U_b$ . The above nondimensionalization results in a dimensionless parameter of  $Re = U_b H / \nu$ . The Reynolds number of  $Re = 6760$  is considered in this study.

A two-step time-split scheme is used to advance the flow field. This scheme is based on the previous works of Kim and Moin (1985) and Zang et al. (1994). First the velocity is advanced from time level 'n' to an intermediate level '\*' by solving the advection–diffusion equation without the pressure term. In the advection–diffusion step, the nonlinear terms are treated explicitly using third-order Adams–Bashforth scheme. The diffusion terms are treated implicitly using Crank–Nicolson scheme. Then the Poisson equation for pressure, which is derived by using mass conservation, is solved fully implicitly. Once the pressure is obtained, the final divergence-free velocity field at 'n+1' is obtained with a pressure-correction step.

The central difference scheme with the second-order accuracy based on the finite volume method is used for the spatial discretization. Additionally, a second-order linear or bilinear interpolation scheme is applied to satisfy the no-slip condition on the immersed boundary. Further details of the immersed boundary method are given in Kim et al. (2001).

The computational domain and the wave dimensions are shown in Fig. 1(a). The two-dimensional wave profile is given by  $h = \alpha \cos(2\pi x/\lambda)$ , where  $h$  is the vertical height with a zero mean value,  $\alpha$  is the wave amplitude and  $\lambda$  is the wavelength. The wave amplitude to wavelength ratio  $\alpha/\lambda$  has changed in five cases having the values 0.01, 0.02, 0.03, 0.04 and 0.05. The computational domain size is  $2\lambda \times 1.1\lambda \times \lambda$  in  $x$ ,  $y$  and  $z$  directions, respectively.

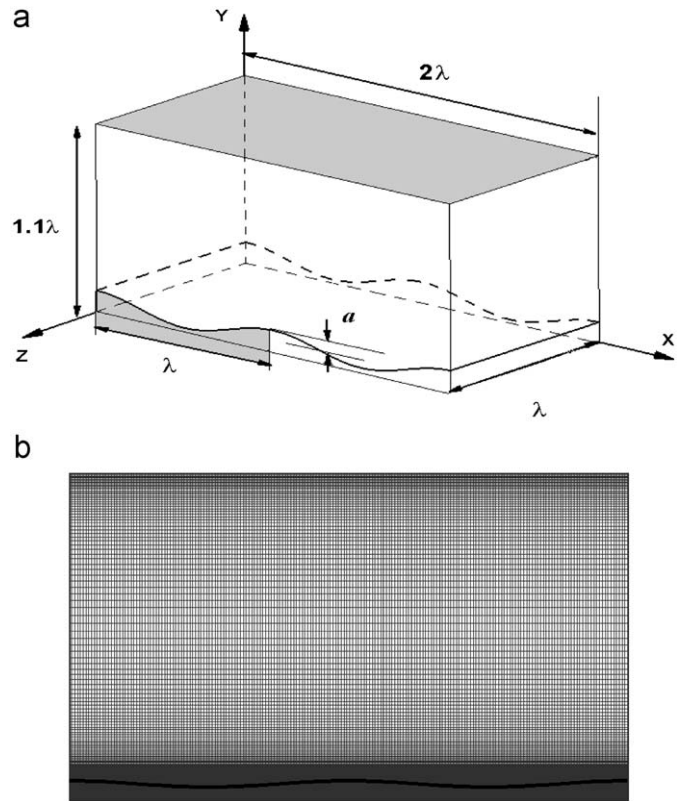


Fig. 1. (a) Computational domain and coordinate system and (b) grid system.

The driving pressure gradient is adjusted to keep constant mass flow rate in the  $x$ -direction in all simulations. The no-slip boundary conditions are enforced at both walls and the periodic boundary conditions are assigned in the streamwise ( $x$ ) and spanwise ( $z$ ) directions.

All simulations in the present study have used  $250 \times 150 \times 100$  grid points in the streamwise, spanwise and wall-normal directions, respectively. Uniform meshes have been used in the streamwise and spanwise directions, while the wall-normal direction uses a hyperbolic tangent distribution to account for the high gradients near the walls. The fine grid is uniformly distributed within the wave to capture the thin boundary layers, while a hyperbolic tangent distribution is in the outer regions. Fig. 1(b) shows the typical grid distribution over the computational domain. In order to consider the variation of the wave amplitude, the number of grid points used in the  $y$ -direction is tuned to maintain the dense resolution near the wave. For the largest wave amplitude of  $\alpha/\lambda = 0.05$  considered in this study, the grid independence of the solution has been confirmed with additional simulations on the finer grids ( $350(x) \times 200(y) \times 100(z)$ ) changing the body forces by less than about 0.3%. The condition of  $CFL < 0.15$  is chosen to determine the nondimensional time step used in the present calculations.

## 3. Results and discussion

### 3.1. Flow characteristics over wave with $\alpha/\lambda = 0.05$

The instantaneous and mean (time- and spanwise-averaged) flow fields in the  $x$ - $y$  plane are shown in Figs. 2(a) and (b),

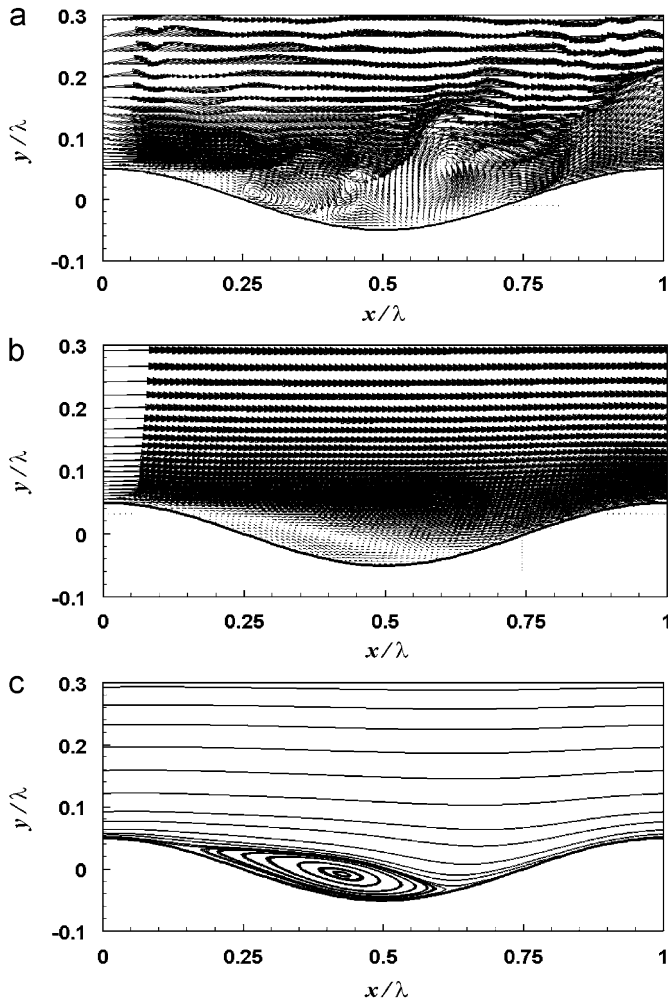


Fig. 2. (a) Instantaneous, (b) time- and spanwise-averaged velocity vectors and (c) time- and spanwise-averaged streamlines near the wavy surface in the  $x$ - $y$  plane at the middle of the spanwise length.

respectively. The separated shear flow located between the crests is clearly shown in Fig. 2(a), which is far more complicated with many intermediate and small-scale components with the strong spatial and temporal dependence. Careful observation along the wavy wall reveals what appear to be wall-layer vortices, arising from the instability of the boundary layers. Time-resolved movies of the velocity vector field as well as the associated vorticity fields have been made even though not shown in here and they display the complex dynamics far more clearly. The interruption of the shear layers by the velocity bursts described as the large eruptions from the trough region is clearly observed in Fig. 2(a), which has also been observed by Kuzan (1986)'s experiment and Cherukat et al. (1998)'s computation.

After the flow has been averaged for long time and over the homogeneous spanwise direction, only one large cell corresponding to the recirculation by the separation is appeared as shown in Figs. 2(b) and (c). One of the important characteristics of mean flow in the wavy channel is the separated zone bounded by the detachment and reattachment points.

The separation and reattachment points are roughly estimated from the mean streamlines in Fig. 2(c). Also, by following the common definition of these points where the wall shear stress disappears, the locations of the separation and reattachment points are more precisely found as  $x/\lambda = 0.14$  and  $x/\lambda = 0.62$ ,

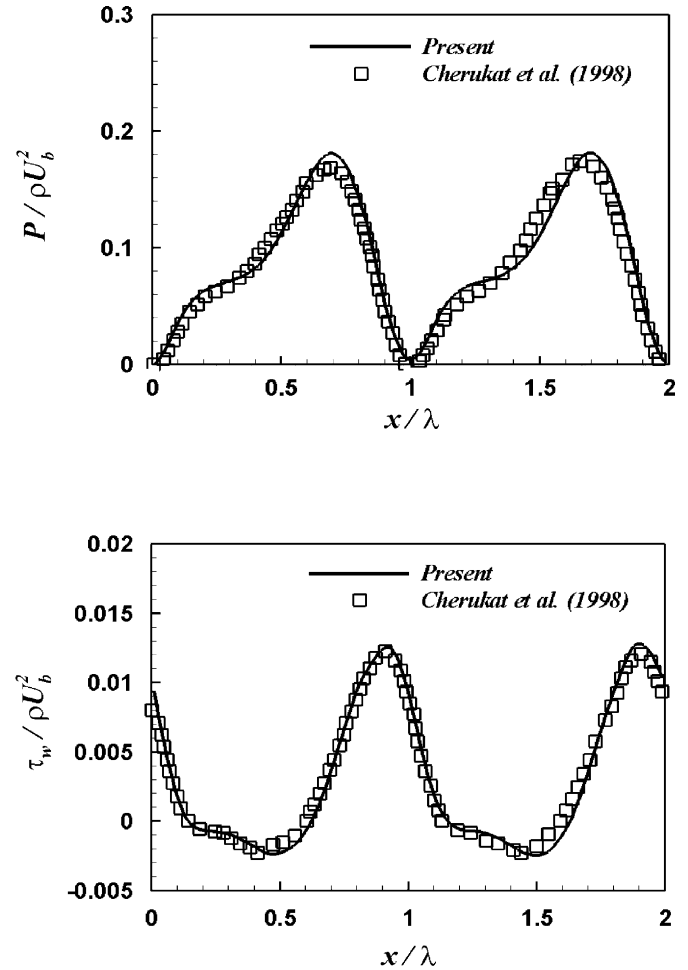


Fig. 3. (a) Comparison of mean pressure and (b) shear stress at wavy wall normalized by  $\rho U_b^2$ .

respectively, which can be clarified by the distribution of the shear stress along the wavy wall in Fig. 3(a). These locations are in good agreement with those of DNS results of Maaß and Schumann (1996) and Cherukat et al. (1998) which showed two locations of  $x/\lambda = 0.14$  and  $x/\lambda = 0.6$  corresponding to the detachment and reattachment positions, respectively.

As well known, when a turbulent boundary layer undergoes an adverse pressure gradient, the flow near the wall decelerates until some backflow occurs; a massive reversed flow follows. Some of the fluid elements with high momentum locally penetrate into the separated zone. This makes the detachment and reattachment zones highly three-dimensional.

The mean pressure and shear stress distributions along the wavy wall are plotted in Figs. 3(a) and (b), respectively, where present results are compared with those of Cherukat et al. (1998). The results agree very well with DNS results of Cherukat et al. (1998). The shear stress reaches to a minimum at  $x/\lambda \sim 0.47$  and rapidly increases to its maximum value at  $x/\lambda \sim 0.92$ . Flow over a wavy surface undergoes large adverse and favorable pressure gradients induced by the waves. The maximum and minimum values of the pressure occur at  $x/\lambda \sim 0.68$  and  $x/\lambda = 1$ , respectively. This variation behavior is in good agreement with the results of Cherukat et al. (1998)'s computation and Buckles et al. (1984)'s experiment.

The variation of the mean streamwise velocity and the mean wall-normal velocity along the streamwise direction plays a role

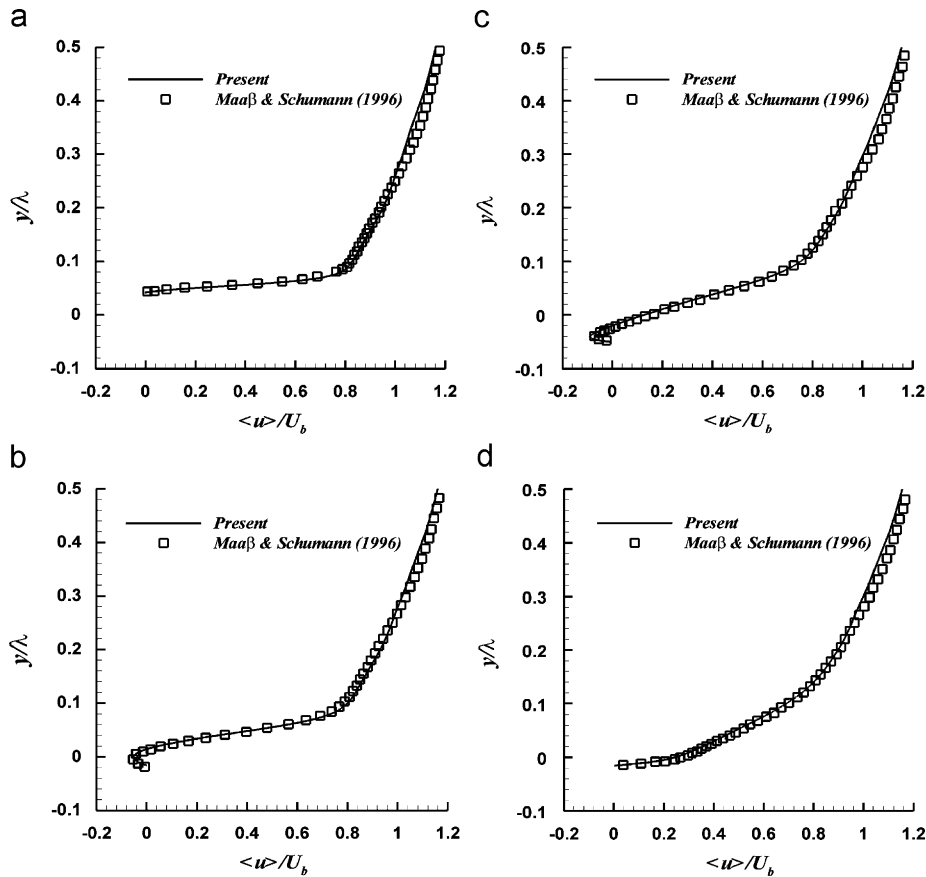


Fig. 4. Mean streamwise velocity profiles at different streamwise locations; (a)  $x/\lambda = 0.1$ , (b)  $x/\lambda = 0.3$ , (c)  $x/\lambda = 0.5$  and (d)  $x/\lambda = 0.7$ .

in predicting the recirculation area bounded by the separation and reattachment points. Thus, the profiles of the mean streamwise and wall-normal velocities at four different streamwise locations within one wave are presented in Figs. 4 and 5, respectively, where present results are also compared with the previous numerical results of Maaß and Schumann (1996).

At  $x/\lambda = 0.1$  just after the wave crest in Fig. 4(a), the values of the streamwise velocities have only positive sign even near the wave surface, since this location is outside of the recirculation zone as early shown in Fig. 2(c). The attached flow moves downward with strong pressure gradient, following the reattachment on the previous wave. Accordingly, the negative wall-normal velocity near the wave surface appears, as shown in Fig. 5(a).

At  $x/\lambda = 0.3$  and  $0.5$ , the flow undergoes the recirculation after it separated owing to the adverse pressure, resulting in the appearance of small negative streamwise velocity as shown in Figs. 4(b) and (c), respectively. For  $x/\lambda = 0.3$  in the downhill, the wall-normal velocity near the wavy surface has the positive velocity as shown in Fig. 5(b), because the fluid is pushed upward along the wavy surface by the reversed flow.

Further downstream, the flow encounters a favorable pressure gradient, the near-wall flow accelerates. At  $x/\lambda = 0.7$ , a negative streamwise velocity disappeared as shown in Fig. 4(d), which indicates the flow reattached already. Beyond the reattachment point, the fluid is pushed upward by the wavy surface as shown in Figs. 2(b and c), which induces only the positive wall-normal velocities at this location as shown in Fig. 5(d).

As shown in Fig. 6, the mean turbulent kinetic energy profiles at different streamwise locations corresponding to Figs. 4 and 5 also agree well with previous numerical results of Maaß and Schumann (1996). As we move from the crest to the trough, the mean turbulent kinetic energy near the wave wall region increases generally. The peak of the mean turbulent kinetic energy locates at  $x/\lambda = 0.5$  and decreases with increasing  $x/\lambda$  in the uphill, which can be clarified by Figs. 6(c) and (d).

In conclusion, the present prediction is in exact agreement and fully consistent with the previous observations (Maaß and Schumann, 1996; Cherukat et al., 1998; Buckles et al., 1984; Balaras, 2004).

### 3.2. Effect of wave amplitude

The instantaneous flow fields in the  $x$ - $y$  plane at the middle of the spanwise domain for the five different wave amplitudes of  $\alpha/\lambda = 0.01, 0.02, 0.03, 0.04$  and  $0.05$  are shown in Figs. 7(a–e), respectively. The grid resolution employed in the present DNS is much finer than what is shown in Fig. 7, where the resolution has been decreased to improve the clarity of visualization.

The smallest wave amplitude of  $\alpha/\lambda = 0.01$  considered in this study does not cause the flow separation to form the recirculation in the valley as shown in Fig. 7(a), regardless of the spanwise direction. When  $\alpha/\lambda = 0.02$ , small recirculating flow occurs near the wave trough as shown in Fig. 7(b) and has the dependence on the spanwise direction (even not shown here for sake of brevity). As expected, with increasing  $\alpha/\lambda$ , the flow is earlier separated and

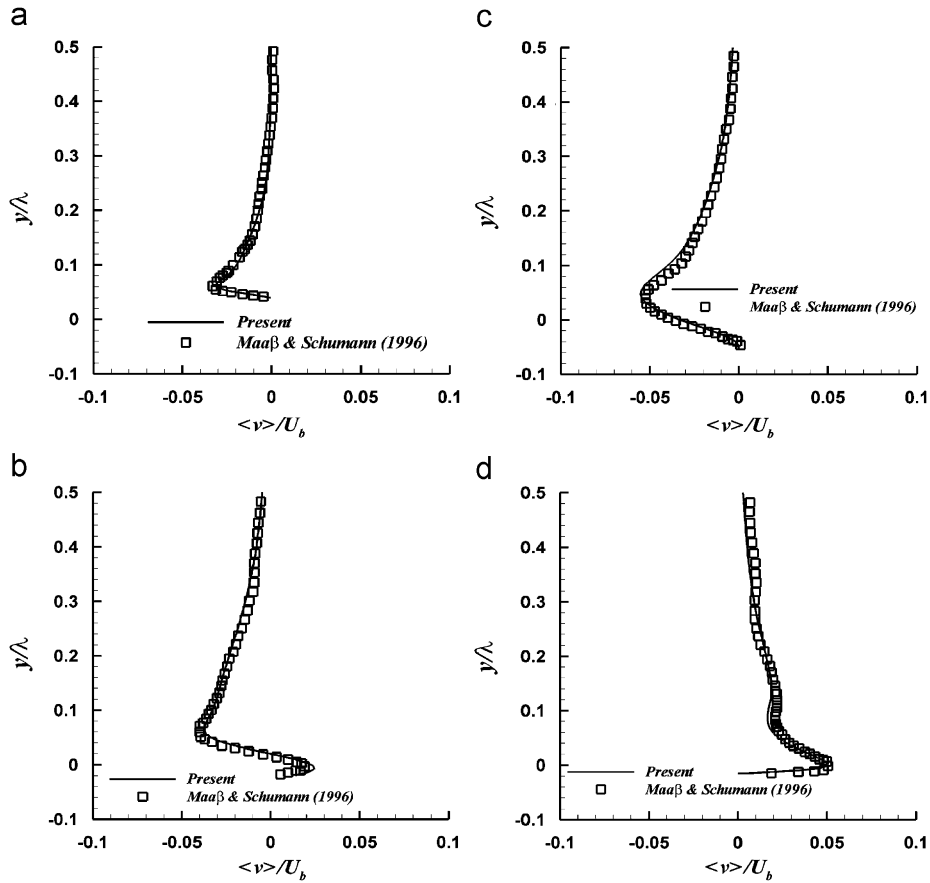


Fig. 5. Mean wall-normal velocity profiles at different streamwise locations; (a)  $x/\lambda = 0.1$ , (b)  $x/\lambda = 0.3$ , (c)  $x/\lambda = 0.5$  and (d)  $x/\lambda = 0.7$ .

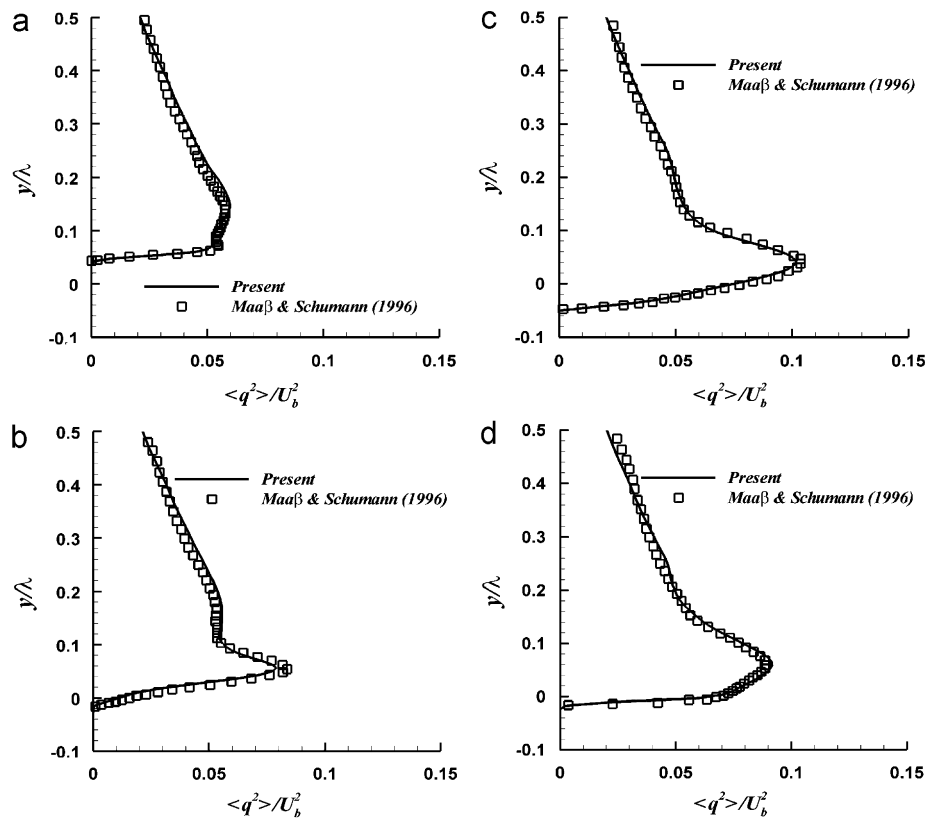
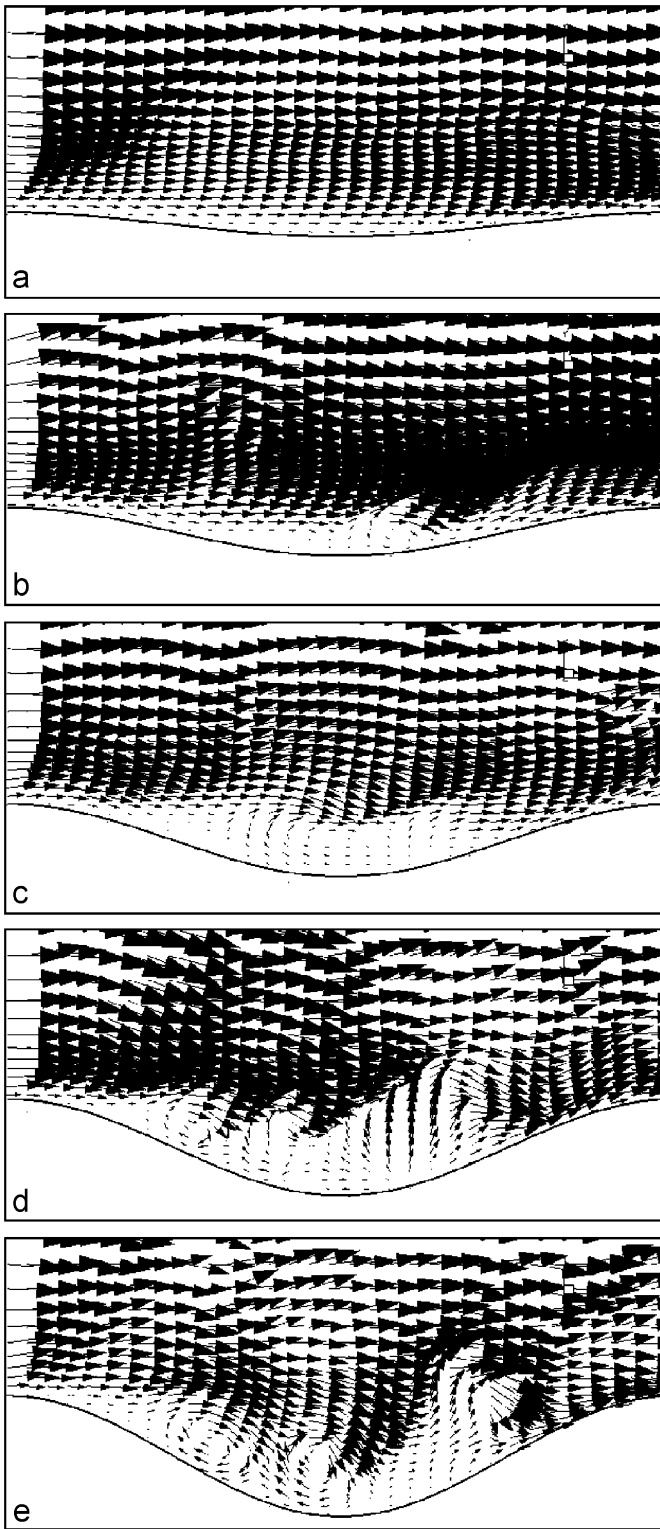


Fig. 6. Mean turbulent kinetic energy profiles at different streamwise locations; (a)  $x/\lambda = 0.1$ , (b)  $x/\lambda = 0.3$ , (c)  $x/\lambda = 0.5$  and (d)  $x/\lambda = 0.7$ .



**Fig. 7.** Instantaneous flow fields in the  $x$ - $y$  plane at the middle of the spanwise domain for the five different wave amplitudes; (a)  $\alpha/\lambda = 0.01$ , (b)  $\alpha/\lambda = 0.02$ , (c)  $\alpha/\lambda = 0.03$ , (d)  $\alpha/\lambda = 0.04$  and (e)  $\alpha/\lambda = 0.05$ . The grid resolution employed in the present DNS is much finer than what is shown above, where the resolution has been decreased to improve the clarity of visualization.

forms the series of vortices with the stronger strength, which is clarified by observing Figs. 7(c)–(e), corresponding to cases of  $\alpha/\lambda = 0.03$ – $0.05$ .

Fig. 8 shows the iso-surfaces of instantaneous streamwise and spanwise vortices near the wavy surface for the five different wave amplitudes of  $\alpha/\lambda = 0.01$ ,  $\alpha/\lambda = 0.02$ ,  $\alpha/\lambda = 0.03$ ,  $\alpha/\lambda = 0.04$  and  $\alpha/\lambda = 0.05$ . For  $\alpha/\lambda = 0.01$ , the streamwise vorticity corresponding to the strength of  $\pm 20$  is nearly not observed in the region near the wave. The spanwise vortices emerged from the crest smoothly elongate along the downstream direction and pass over the trough, as shown in Fig. 8(a).

In the case of  $\alpha/\lambda = 0.02$ , the sparse distribution of small streamwise vortices appear near the uphill. The spanwise vortices become thinner and slightly inclines into the trough, when the flow passes over the trough as shown in Fig. 8(b). These variations of the streamwise and the spanwise vortices compared with the lower amplitude of  $\alpha/\lambda = 0.01$  is associated with the interaction of the shear layers with the weak recirculation flow appeared near the trough as early shown in Fig. 7(b).

In the cases of  $\alpha/\lambda = 0.03$ ,  $0.04$  and  $0.05$  as shown in Figs. 8(c)–(e), respectively, the spanwise vortices associated with the thin accelerating boundary layers initially are emerged from any in the upslope area of the wave. Then, they travel over the following crest and continuously move forward into the shear layer above the separation region. Eventually, they break up and spread out, forming the cluster of vortices over the trough. Mainly, the streamwise vortices appear over the trough and especially develop over the upslope area. These evolution and distribution of vortical structures in the near wavy wall region are consistent with the findings of previous researches (De Angelis et al., 1997; Cherukat et al., 1998; Balaras, 2004). In particular, De Angelis et al. (1997) well discussed the mechanism of the evolution of the turbulent structure in the near wavy wall region. As expected, with increasing  $\alpha/\lambda$ , both vortices distribute densely and widely in the near wavy wall region owing to the early separation and later reattachment, which can be clarified by comparing Figs. 8(c)–(e) corresponding to cases of  $\alpha/\lambda = 0.03$ ,  $0.04$  and  $0.05$ , respectively. The variation of the locations of the separation and reattachment along the  $\alpha/\lambda$  will be discussed later.

Fig. 9 shows the mean velocity vectors with superimposed mean streamlines for different wave amplitudes. In cases of  $\alpha/\lambda = 0.01$  and  $0.02$ , the reverse flows in the mean flow field are not observed in Figs. 9(a) and (b), respectively. For  $\alpha/\lambda = 0.02$ , it is worthwhile noting that the recirculating flow has been observed in the instantaneous flow early shown in Fig. 7(b). However, as expected, owing to the time-dependent jitter in the position of the small vortices near the trough, the mean vortical structure decays with the advancing time average and eventually the mean reverse flow does not exist. When the wave amplitude is  $\alpha/\lambda = 0.03$ , the reverse flow appears as shown in Fig. 9(c). As  $\alpha/\lambda$  increases, the size of recirculation area becomes bigger owing to the earlier separation and the more delayed reattachment, as shown in Figs. 9(c)–(e).

Fig. 10 shows more precisely the variation of the separation and reattachment locations according to the wave amplitude. As above mentioned in Fig. 2(c), the locations of the separation and reattachment points are estimated, using the mean streamlines in Fig. 9 and also the distribution of the shear stress along the wavy wall in Fig. 13(b). Among the wave amplitudes considered in this study, the mean recirculating flow appears from  $\alpha/\lambda = 0.03$ . As  $\alpha/\lambda$  increases from  $0.03$  to  $0.05$ , the location of separation is closer to the crest with the values of  $x/\lambda = 0.22$ ,  $0.17$  and  $0.14$ . The reattachment point is closer to the following crest with the values of  $x/\lambda = 0.58$ ,  $0.6$  and  $0.62$ , with increasing  $\alpha/\lambda$  from  $0.03$  to  $0.05$ .

The onset and modification of the mean reverse flow according to the wave amplitude is also reinforced with the contours of mean streamwise and wall-normal velocities for the five different

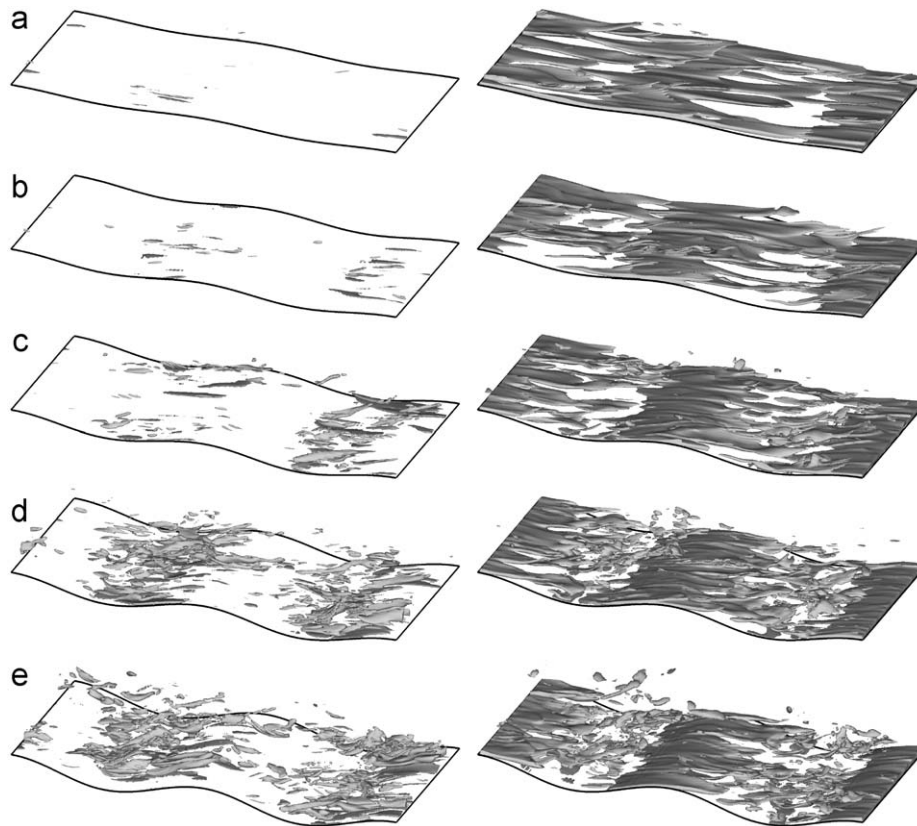


**Fig. 8.** Iso-surfaces of instantaneous streamwise vorticity (left column) and spanwise vorticity (right column) for the five different wave amplitudes; (a)  $\alpha/\lambda = 0.01$ , (b)  $\alpha/\lambda = 0.02$ , (c)  $\alpha/\lambda = 0.03$ , (d)  $\alpha/\lambda = 0.04$  and (e)  $\alpha/\lambda = 0.05$ .

wave amplitudes in Fig. 11. Regardless of the wave amplitude, the mean streamwise velocity forms the boundary layer near the crest thinner than that near the trough, which is certified by denser contours near the crest thinner than that near the trough, as shown in Figs. 11(a–e).

When the separation occurs from  $\alpha/\lambda = 0.03$ , as shown in Fig. 11(c), the negative values of the mean streamwise velocity appear in the region corresponding to the recirculation area observed in Figs. 9 and 10. This recirculation area occupied by the negative streamwise velocity increases with increasing  $\alpha/\lambda$  as shown in Figs. 11(c)–(e), which is consistent with corresponding Figs. 9(c)–(e).

As  $\alpha/\lambda$  increases, especially in cases of  $\alpha/\lambda = 0.03$ , 0.04 and 0.05 forming the reverse flow, the thinner boundary layer induced from the reattachment point grows and accelerates under strong favorable pressure gradients as the flow moves over the next crest.

In cases of  $\alpha/\lambda = 0.01$  and 0.02 where the mean reverse flow is not observed, the contours of mean wall-normal velocity show the negative values in the front (first) half of the wave and positive ones in the other half of the wave, since the flow moves downward and upward alternatively following to the wave geometry. The negative and positive peaks appear at  $x/\lambda \sim 0.26$  and  $x/\lambda \sim 0.82$ , respectively. The positive wall-normal velocity is much larger than the negative one as shown in Figs. 11(a) and (b), because the flow accelerates on the uphill and decelerates on the downhill.

When the mean reverse flow occurs from  $\alpha/\lambda = 0.03$ , the positive wall-normal velocity appears near the trough in the first half of the wave. With further increase in  $\alpha/\lambda$ , the area having the positive wall-normal velocity extends, resulting in pushing the area with the negative one upward and simultaneously towards

the next crest. Consequently, the area with positive wall-normal velocity in the uphill region is squeezed with increasing  $\alpha/\lambda$ , as shown in Figs. 11(c)–(e). The location of the maximum wall-normal velocity is pushed upward, reaching to  $x/\lambda \sim 0.85$  when  $\alpha/\lambda = 0.05$ .

Fig. 12 shows the contours of turbulent kinetic energy,  $\langle q^2 \rangle / U_b^2$  and the Reynolds shear stress,  $\langle u'v' \rangle / U_b^2$  for the five different wave amplitudes. Generally, the contours of the turbulent kinetic energy form denser distribution near the downstream from the trough than that near the upstream region from the trough. This pattern of turbulent kinetic energy distribution along the wavy surface is more apparent with increasing  $\alpha/\lambda$  in company with the augmentation of its magnitude. For  $\alpha/\lambda = 0.01$ , the maximum of turbulent kinetic energy is located at slightly downstream from the trough. As  $\alpha/\lambda$  increases, the location of the maximum turbulent kinetic energy is closer to the trough. In cases of  $\alpha/\lambda = 0.03$ , 0.04 and 0.05 showing the mean reverse flow, the vertical location of the maximum turbulent kinetic energy is approximately at the height of the crest corresponding the wavy amplitude over the trough. The Reynolds shear stress has a maximum approximately at the same location as the turbulent kinetic energy, regardless of the wave amplitude. Also, the contours of Reynolds shear stress show the similar distribution as the turbulent kinetic energy, except the uphill region where the negative values of Reynolds shear stress appear, because the Reynolds shear stress is calculated in a Cartesian coordinate. Especially for  $\alpha/\lambda = 0.05$ , the present results of turbulent kinetic energy and the Reynolds shear stress distribution are full, consistent with the previous observation of Balaras (2004).

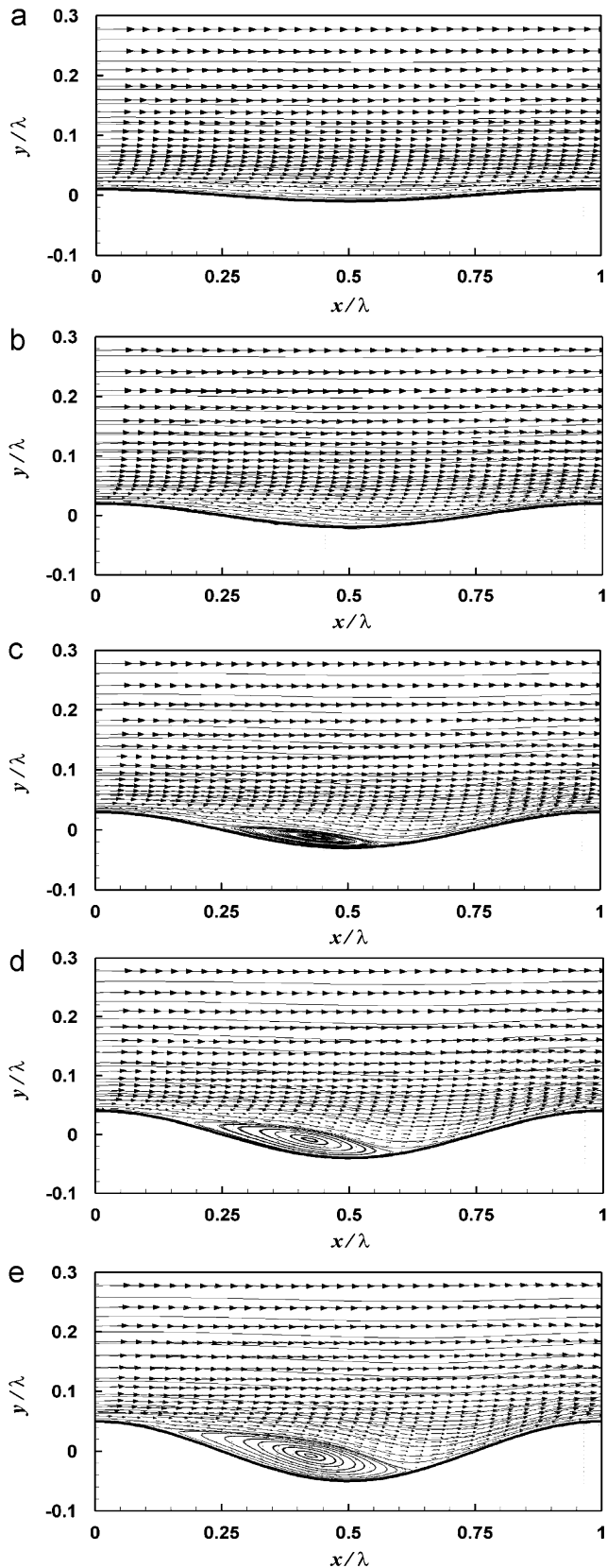


Fig. 9. Mean velocity vectors with superimposed the mean streamlines for five different wave amplitudes; (a)  $\alpha/\lambda = 0.01$ , (b)  $\alpha/\lambda = 0.02$ , (c)  $\alpha/\lambda = 0.03$ , (d)  $\alpha/\lambda = 0.04$  and (e)  $\alpha/\lambda = 0.05$ .

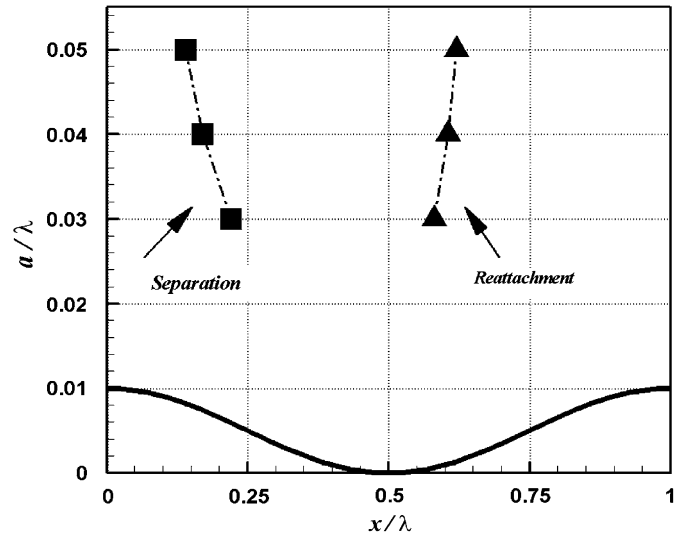


Fig. 10. Locations of separation and reattachment for three different wave amplitudes of  $\alpha/\lambda = 0.03$ ,  $\alpha/\lambda = 0.04$  and  $\alpha/\lambda = 0.05$ .

Fig. 13 shows the variations of time- and spanwise-averaged pressure and shear stress along the wavy wall for the different wave amplitudes. Flow over a wavy surface experiences larger adverse and favorable pressure gradients with increasing  $\alpha/\lambda$ . In the cases of  $\alpha/\lambda = 0.03, 0.04$  and  $0.05$  forming the reverse flow, the inflectional point of pressure is observed on the first half of wave, which has been also found in De Angelis et al. (1997)'s computation. As  $\alpha/\lambda$  increases, the location of a maximum pressure becomes more distant from the trough, whereas that of a minimum pressure is independent of  $\alpha/\lambda$  and is at  $x/\lambda \sim 1$ , as shown in Fig. 13(a).

The shear stress profile becomes sharper with increasing  $\alpha/\lambda$ . The negative values of shear stress appears from the  $\alpha/\lambda = 0.03$  and extend to wider range with increasing  $\alpha/\lambda$ , as shown in Fig. 13(b), which is associated with the reverse flow observed already in the mean flow fields. The location of a maximum shear stress becomes closer to the crest and that of a minimum pressure becomes closer to the trough.

Fig. 14 shows the drag coefficients as a function of the wave amplitude, where the total drag coefficient ( $C_T$ ) is composed of the pressure drag coefficient ( $C_P$ ) and the friction drag coefficient ( $C_F$ ). Here, the value of  $C_F$  of the plane channel marked as the dashed line to clearly identify the waviness effect. The characteristics of drag forces exerted on the wavy surface are investigated in terms of the drag coefficients which are nondimensionalized by surface plane area. The pressure drag coefficient,  $C_P$  increases rapidly with increasing  $\alpha/\lambda$ . In contrast, the friction drag coefficient,  $C_F$  shows the increase and decrease behavior according to  $\alpha/\lambda$ .  $C_F$  has a maximum at  $\alpha/\lambda = 0.03$ , where the mean reverse flow appears and decreases with continuously increasing  $\alpha/\lambda$ . For  $\alpha/\lambda = 0.05$ ,  $C_F$  is smaller than that of the plane channel. In the range of  $0.01 \leq \alpha/\lambda \leq 0.03$ ,  $C_F$  is larger than  $C_P$ . For  $\alpha/\lambda \geq 0.04$ , the situation reversed.

#### 4. Conclusions

The present study has numerically investigated the effect of the wave amplitude on the turbulent flow. In a second-order accurate finite volume method, an immersed boundary method is

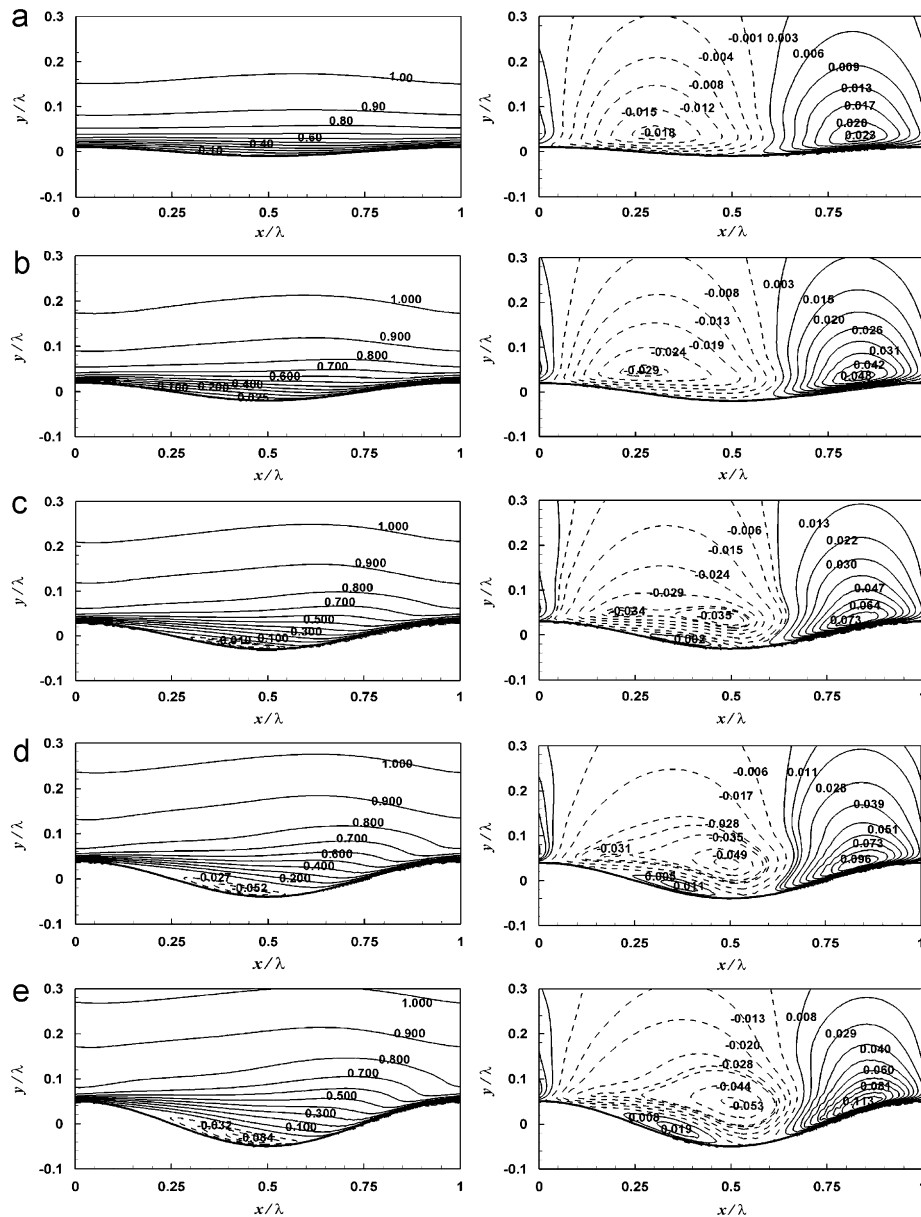


**Fig. 11.** Mean contours of streamwise velocity (left column) and wall-normal velocity (right column) for the five different wave amplitudes; (a)  $\alpha/\lambda = 0.01$ , (b)  $\alpha/\lambda = 0.02$ , (c)  $\alpha/\lambda = 0.03$ , (d)  $\alpha/\lambda = 0.04$  and (e)  $\alpha/\lambda = 0.05$ .

adopted to handle the wavy surface in the Cartesian coordinates. Comparisons with the published references show excellent agreement in detecting the locations of the separation and reattachment, the mean pressure and shear stress, the mean velocities and the mean turbulent kinetic energy.

The flow has been computed for five different wave ratios of 0.01, 0.02, 0.03, 0.04 and 0.05 at one bulk Reynolds number of 6760.

For  $\alpha/\lambda = 0.01$ , the separation has not occurred. When  $\alpha/\lambda = 0.02$ , in the instantaneous flow field, the appearance of the separation causes the flow to undergo the recirculation in the valley. Further increasing  $\alpha/\lambda$ , the flow is earlier separated and forms the series of vortices with the stronger strength. The mean recirculating flow appears from  $\alpha/\lambda = 0.03$ . As  $\alpha/\lambda$  increases from 0.03 to 0.05, the location of separation is closer to the crest and the reattachment point is closer to the following crest. The onset

and modification of the mean reverse flow according to the wave amplitude has been reinforced with the contours of mean streamwise and wall-normal velocities.

The turbulent kinetic energy formed denser distribution near the downstream from the trough than that near the upstream region from the trough. As  $\alpha/\lambda$  increases, this pattern of turbulent kinetic energy distribution is more significant with the augmentation of its magnitude. The location of the maximum turbulent kinetic energy is closer to the trough with increasing  $\alpha/\lambda$ . When the mean reverse flow appears, the vertical location of the maximum turbulent kinetic energy is approximately at the height of the crest. The Reynolds shear stress shows the similar distribution as the turbulent kinetic energy.

As  $\alpha/\lambda$  increases, the location of a maximum pressure becomes more distance from the trough, whereas that of a minimum

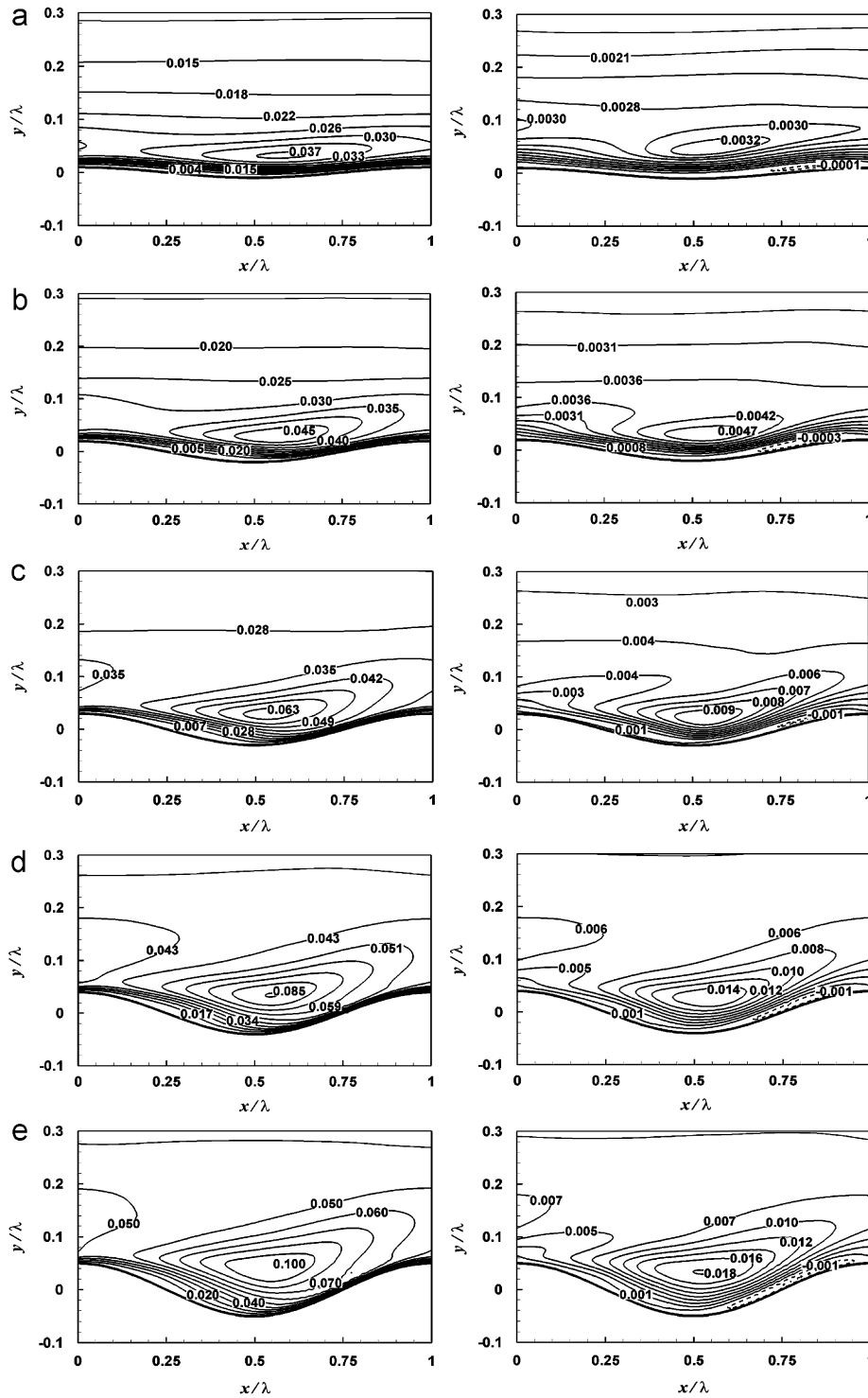


**Fig. 12.** Contours of turbulent kinetic energy,  $\langle q^2 \rangle / U_b^2$  (left column) and the Reynolds shear stress,  $\langle u'v' \rangle / U_b^2$  (right column) for the five different wave amplitudes; (a)  $\alpha/\lambda = 0.01$ , (b)  $\alpha/\lambda = 0.02$ , (c)  $\alpha/\lambda = 0.03$ , (d)  $\alpha/\lambda = 0.04$  and (e)  $\alpha/\lambda = 0.05$ .

pressure is independent of  $\alpha/\lambda$ . The location of a maximum shear stress becomes closer to the crest and that of a minimum pressure becomes closer to the trough. The negative values of shear stress appears from the  $\alpha/\lambda = 0.03$  and occupy the wider range with increasing  $\alpha/\lambda$ , which is associated with the mean reverse flow.

The pressure drag coefficient shows the increase behavior with increasing  $\alpha/\lambda$ . However, the friction drag coefficient shows the increase and decrease behavior according to  $\alpha/\lambda$ . The friction drag coefficient has a maximum at  $\alpha/\lambda = 0.03$  and diminished with continuously increasing  $\alpha/\lambda$ .

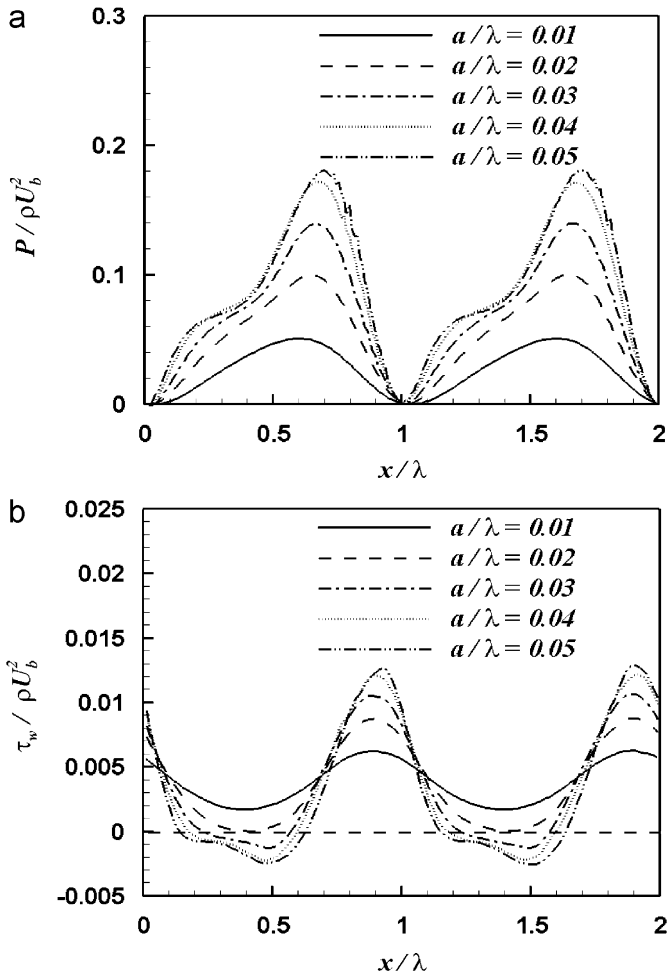


Fig. 13. Distributions of (a) mean pressure and (b) mean shear stress along the wavy wall for five different wave amplitudes.

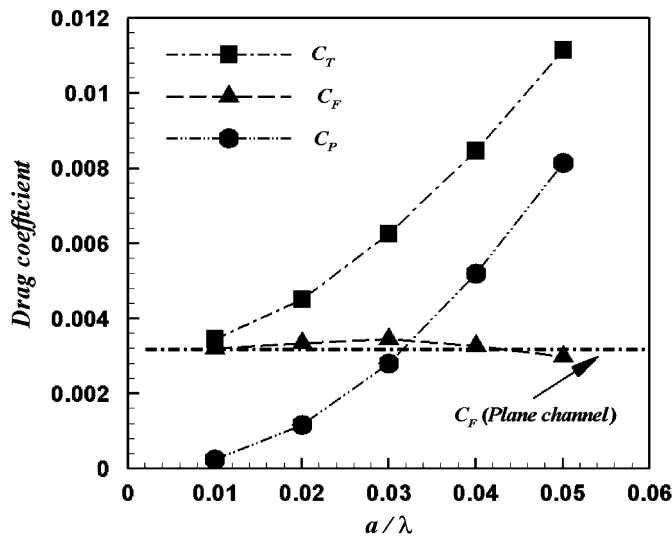


Fig. 14. Drag coefficients as a function of the wave amplitude, where the total drag coefficient ( $C_T$ ) is composed of the pressure drag coefficient ( $C_P$ ) and the friction drag coefficient ( $C_F$ ). Here, the value of  $C_F$  of the plane channel marked as solid line to clearly identify the waviness effect.

### Acknowledgment

This work was supported by the Advanced Ship Engineering Research Center (ASERC) of Pusan National University through Korea Science and Engineering Foundation.

### References

Balaras, E., 2004. Modeling complex boundaries using an external force field on fixed Cartesian grids in large-eddy simulations. *Computers and Fluids* 33, 375–404.

Buckles, J., Hanratty, T.J., Adrian, R.J., 1984. Turbulent flow over a large-amplitude wavy surface. *Journal of Fluid Mechanics* 140, 27–44.

Cherukat, P., Na, Y., Hanratty, T.J., 1998. Direct numerical simulation of a fully developed turbulent flow over a wavy wall. *Theoretical and Computational Fluid Dynamics* 11, 109–134.

De Angelis, V., Lombardi, P., Banerjee, S., 1997. Direct numerical simulation of turbulent flow over a wavy wall. *Physics of Fluids* 9, 2429–2442.

Hudson, J.D., Dykhno, L., Hanratty, T.J., 1996. Turbulence production in flow over a wavy wall. *Experiments in Fluids* 20, 257–265.

Kim, J., Kim, D., Choi, H., 2001. An immersed-boundary finite volume method for simulations of flow in complex geometries. *Journal of Computational Physics* 171, 132–150.

Kim, J., Moin, P., 1985. Application of a fractional step method to incompressible Navier–Stokes equations. *Journal of Computational Physics* 59, 308–323.

Kuzan, J.D., 1986. Velocity measurements for turbulent-separated and near-separated flow over solid waves. Ph.D. Thesis, University of Illinois, Urbana, IL.

Kuzan, J.D., Hanratty, T.J., Adrian, R.J., 1989. Turbulent flows with incipient separation over solid waves. *Experiments in Fluids* 7, 88–98.

Maaß, C., Schumann, U., 1996. Direct numerical simulation of separated turbulent flow over a wavy boundary. In: Hirschel, E.H. (Ed.), *Flow simulation with high-performance computers. Notes on numerical fluid mechanics*, vol. 52. pp. 227–241.

Zang, Y., Street, R.L., Koseff, J.R., 1994. A non-staggered grid, fractional step method for time-dependent incompressible Navier–Stokes equations in curvilinear coordinates. *Journal of Computational Physics* 114, 18–33.

Zilker, D.P., Hanratty, T.J., 1979. Influence of the amplitude of a solid wavy wall on a turbulent flow. Part 2. Separated flows. *Journal of Fluid Mechanics* 90, 257–271.